Received: 30 April 2018 | Revised: 19 July 2018 | Accepted: 10 August 2018

DOI: 10.1002/mrm.27514

RAPID COMMUNICATION

Magnetic Resonance in Medicine

Creatine and phosphocreatine mapping of mouse skeletal muscle by a polynomial and Lorentzian line-shape fitting CEST method

Lin Chen[1,2] | **Peter B. Barker**[1,2] | **Robert G. Weiss**[2,3] | **Peter C. M. van Zijl**[1,2] | **Jiadi Xu**[1,2]

[1]F.M. Kirby Research Center for Functional Brain Imaging, Kennedy Krieger Research Institute, Baltimore, Maryland

[2]Russell H. Morgan Department of Radiology and Radiological Science, Johns Hopkins University School of Medicine, Baltimore, Maryland

[3]Division of Cardiology, Department of Medicine, Johns Hopkins University School of Medicine, Baltimore, Maryland

Correspondence
Jiadi Xu, Kennedy Krieger Institute, Johns Hopkins University School of Medicine, 707 N. Broadway, Baltimore, MD 21205.
Email: xuj@kennedykrieger.org

Funding information
NIH (R01EB015032, P41EB015909, and R01HL63030).

Purpose: To obtain high-resolution Cr and PCr maps of mouse skeletal muscle using a polynomial and Lorentzian line-shape fitting (PLOF) CEST method.

Methods: Wild-type mice and guanidinoacetate N-methyltransferase–deficient (GAMT-/-) mice that have low Cr and PCr concentrations in muscle were used to assign the Cr and PCr peaks in the Z-spectrum at 11.7 T. A PLOF method was proposed to simultaneously extract and quantify the Cr and PCr by assuming a polynomial function for the background and 2 Lorentzian functions for the CEST peaks at 1.95 ppm and 2.5 ppm.

Results: The Z-spectra of phantoms revealed that PCr has 2 CEST peaks (2 ppm and 2.5 ppm), whereas Cr only showed 1 peak at 2 ppm. Comparison of the Z-spectra of wild-type and GAMT-/- mice indicated that, contrary to brain, there was no visible protein guanidinium peak in the skeletal-muscle Z-spectrum, which allowed us to extract clean PCr and Cr CEST signals. High-resolution PCr and Cr concentration maps of mouse skeletal muscle were obtained by the PLOF CEST method after calibration with in vivo MRS.

Conclusions: The PLOF method provides an efficient way to map Cr and PCr concentrations simultaneously in the skeletal muscle at high MRI field.

KEYWORDS

chemical exchange saturation transfer, creatine, guanidinoacetate, guanidinoacetate N-methyltransferase deficiency mouse, magnetization transfer contrast, phosphate guanidinoacetate, phosphocreatine, polynomial and Lorentzian line-shape fitting

1 | INTRODUCTION

Creatine and PCr are 2 primary components of the creatine kinase reaction, arguably the primary energy reserve reaction in muscle,[1,2] in which Cr is phosphorylated to PCr to form a mobilizable reserve of high-energy phosphates.[3] Therefore, quantification of the concentrations and tissue distribution of Cr and PCr are important for understanding cellular chemistry and assessing pathologic alterations. The conventional techniques to quantify tissue concentrations of Cr and PCr are ^{1}H and ^{31}P MRS. ^{1}H MRS enables the measurement of tCr, which consists of Cr and PCr.[4,5] In contrast, ^{31}P MRS is only capable of detecting PCr, as Cr does not contain phosphorus.[6,7] Despite the success of this technique, MRS

quantification is limited by a relatively low SNR and spatial resolution. In addition, MRS techniques have difficulty in detecting PCr and Cr simultaneously.

The development of the CEST method[8–13] provides an opportunity to detect low concentrations of PCr and Cr in tissues.[14,15] One method of Cr CEST uses magnetization transfer ratio asymmetry (MTR_{asym}) analysis (i.e., subtracting the labeling and control images acquired at the 2 symmetric offsets with respect to water resonance).[14–16] This approach is similar to many other CEST applications, such as APT-CEST,[17] GlycoCEST,[18] GluCEST,[19] and gagCEST.[20] However, tissue contains many types of exchangeable protons on both sides of the Z-spectrum, such as the amine protons from proteins and glutamate at 2.5 ppm,[19,21–23] the hydroxyl groups from proteins and Myo-inositol at approximately 1 ppm,[24–26] the relayed nuclear Overhauser effect CEST signals from Cho at –1.6 ppm,[27] and the aliphatic protons in proteins and lipids between –2 ppm and –4 ppm,[20,24,28,29] making asymmetry analysis vulnerable to contaminations from lipids, proteins, semisolid macromolecules, and other metabolites.

Another way of estimating the tissue Cr CEST is by acquiring a full Z-spectrum using a continuous-wave RF irradiation with low saturation power and fitting it by assuming a Lorentzian line-shape for the resonances of each exchanging proton pool, including water, amide, guanidinium, and the relayed nuclear Overhauser effect peaks.[30] This method, however, is still not able to cleanly distinguish the Cr signal from the other CEST signals, such as the amine and aromatic protons at 2 ppm.[31] In addition to the continuous-wave CEST, a pulsed-CEST method dubbed "chemical exchange rotation transfer"[32,33] has been developed to selectively detect slow to intermediate exchanging protons. This method has the potential to selectively map Cr and PCr signals with minor contaminations from proteins[34] that also contain some guanidinium protons resonating at 2 ppm. Recently, a Cr CEST study carried out on guanidinoacetate methyltransferase deficient (GAMT-/-) mouse brain showed that the tCR signal contributes only part of the guanidinium peak at 1.95 ppm,[35] a finding that is consistent with an ex vivo study using homogenous rat brain tissue.[36] Based on these findings, we developed a polynomial and Lorentzian line-shape fitting (PLOF) method to extract and quantify the tCr signal in the brain.[35] This new method is assumed to remove most contaminations to the tCr CEST signal except for a small portion of signal from the protein guanidinium protons.

In the current study, we extend the PLOF method to map the PCr and Cr concentrations simultaneously in mouse skeletal muscle. Although the CEST signals at 2 ppm and 2.5 ppm have been shown to be related to Cr and PCr, the accurate quantification of Cr and PCr still faces several challenges. First, the concentrations of PCr, Cr, and mobile proteins in skeletal muscle are quite different from those in the brain. In previous studies, the lack of an efficient way to extract the PCr and Cr signals from the skeletal muscle Z-spectrum was primarily due to the uncertainty of the amount of the Cr and PCr contributions in the Z-spectrum. In this study, we used GAMT-/- mice to verify the contribution of the Cr and PCr signal to the muscle CEST Z-spectrum. Second, the acquisition parameters to maximize CEST contrast of Cr and PCr in skeletal muscle are significantly different from those for phantom studies due to the abundance of semisolid macromolecular tissue components. In this study, we optimized the saturation power to obtain the maximum CEST contrast of Cr and PCr in skeletal muscle at 11.7 T. Third, the PLOF method is a recently proposed CEST quantification method that has been validated for obtaining high-resolution Cr maps in mouse brain. However, the initial PLOF method used for brain is not suitable for the 2-peak case in this muscle study, in which CEST signal at 2.5 ppm contains the contribution from PCr, whereas CEST signal at 2 ppm contains the contributions from both Cr and PCr. Here we propose an improved PLOF method to resolve this problem and yield both high-resolution Cr and PCr concentration maps.

2 | METHODS

2.1 | Magnetic resonance imaging experiments

All MRI experiments were performed on a horizontal-bore 11.7T Bruker Biospec system (Bruker, Ettlingen, Germany). For the animal studies, a 72-mm quadrature-volume resonator was used as a transmitter and a 4-element (2 × 2) phased array coil was used as a receiver. A 23-mm-volume transceiver coil was used for the phantom studies. Six saturation powers (0. 3 μT, 0.6 μT, 0.8 μT, 1 μT, 1.5 μT, and 2 μT) were used for the optimization of the PCr/Cr CEST signals. According to previous studies, the steady-state condition, at which the CEST signal will not increase with longer saturation length, was determined by the $R_{1\rho}$ values at each saturation power.[35,39,40] Saturation lengths of 4 seconds for 0.3 μT to 0.8 μT power, 3 seconds for 1 μT to 1.5 μT power, and 2 seconds for 2 μT power will reach the steady-state saturation and were applied in the current study. The saturation offsets were swept from –7 ppm to 5 ppm with an increment of 0.2 ppm. Here, –7 ppm was chosen due to the broad peaks from semisolid components with a center frequency in the aliphatic range. A 0.05-ppm increment was used between 1.5 ppm and 2.8 ppm to facilitate the fitting of the PCr/Cr CEST signals. The MR images were acquired using a turbo spin echo sequence with TE = 3.7 ms, turbo spin echo factor = 16, slice thickness =1.5 mm, a matrix size of 64 × 32, and a resolution of 0.25 × 0.25 mm^2. The B_0 field over the mouse brain was adjusted using field mapping and second-order

shimming. The R_1 relaxation of the mouse brain was measured using variable-TR rapid acquisition with refocused echoes (TR = 5.5, 3.0, 1.5, 0.8, 0.5, 0.3 seconds). The in vivo MRS experiments were performed on a voxel of 2 × 2 × 2 mm^3 using a stimulated-echo acquisition mode sequence (TE = 3 ms, Mixing Time (TM) = 10 ms, TR = 2.5 seconds, number of acquisitions NA = 256) following the experimental parameters given previously.[35]

Freshly made phantoms with Cr (5, 10, 20, and 30 mM), PCr (5, 10, 20, and 30 mM), and guanidinoacetate (Gua) (30 mM) solutions were used to investigate the power and concentration dependence of the CEST contributions of guanidinium proton–containing compounds in muscle. Notice that phosphorylated guanidinoacetate (PGua) protons contribute to the CEST Z-spectrum of the GAMT-/- mouse. However, PGua is not commercially available. These three components (Cr, PCr, and Gua) were used to assign the in vivo CEST peaks. All phantoms were prepared in phosphate buffered saline, titrated to pH 7.0. The phantoms were maintained at 37°C during the MRI experiments with an air heater. A calibration phantom with 20-mM Cr mixed with cross-linked bovine serum albumin (BSA) (20% by weight, pH = 7.2) was used for the MRS quantification. The BSA was cross-linked using glutaraldehyde following a previously described procedure.[41] The T_1 relaxation time of water protons in the cross-linked BSA (T_1 = 1.8 seconds) is close to that of mouse muscle (T_1 = 1.9 seconds) at 11.7 T. Although the T_2 value (T_2 = 46 ms) in the cross-linked BSA is higher than that in muscle (T_2 = 26 ms), the effect on the MRS quantification is minimized due to the short TE stimulated-echo acquisition mode method applied.

2.2 | Animal studies

The institutional animal care and use committee approved this study. Three adult female BALB/c mice (14 months) as wild type (WT) mice and 3 GAMT-/- mice (14 months) were used. The tCr of the GAMT-/- mouse muscle is significantly reduced compared with the WT counterpart.[42–46] However, the amount of PGua is still considerable, as confirmed by a ^{31}P MRS study.[42] All animals were induced using 2% vaporized inhaled isoflurane, followed by 1.5% isoflurane during the MRI scan.

2.3 | Creatine and PCr quantification using the 2-peak PLOF method

For the in vivo CEST studies, the observed CEST peak is scaled down by a factor of Z^2 compared with the signal from the phantom,[35] where Z is the normalized value of the steady-state Z-spectrum. This scale-down effect, dubbed the spillover effect, is determined by the tissue macromolecule concentrations and the applied saturation parameters.[40,47–50] The PLOF quantification method based on the $R_{1\rho}$ relaxation theory is robust against the spillover effect.[35] In the current study, a 2-peak PLOF method is designed to extract and quantify the PCr and Cr CEST signals simultaneously. In the framework of the $R_{1\rho}$ relaxation theory, the normalized saturation signal Z^{ss} (i.e., the water saturation signal S normalized by the signal without saturation, S_0) at steady state for each offset is given by[39,40,47]

$$Z^{ss} = \frac{cos^2\theta R_1}{R_{1\rho}} \tag{1}$$

where R_1 is the longitudinal relaxation rate of water and $\theta = tan^{-1}\omega_1/\Delta$ is the tilt angle of the effective magnetization with respect to the z-axis induced by the RF saturation with a nutation frequency of ω_1 and an offset of Δ. The value of $R_{1\rho}$ is the water relaxation rate under RF saturation, which contains the contributions from the effective water relaxation accounting for the direct saturation effect in the Z-spectra and an apparent relaxation term due to all the saturation transfer processes in the tissue.[40]

$$R_{1\rho} = R_{eff} + R_{back} + R_{peak1} + R_{peak2} \tag{2}$$

where $R_{eff} = cos^2\theta R_1 + sin^2\theta R_2$ is the longitudinal relaxation rate of water in the rotating frame without additional solutes. The value of R_{back} is the background pool that includes the water direct saturation, the magnetization transfer contrast (MTC), the aromatic protons, and the other metabolites. The values of R_{peak1} and R_{peak2} are the introduced rotational frame relaxation rates of the 2 targeted CEST peaks. In the current study, these are the peaks at 1.95 ppm (Cr + PCr) and 2.5 ppm (PCr), respectively. The Z-spectrum can be fitted using Eqs. 1 and 2 by assuming R_{peak1} and R_{peak2} as 2 Lorentzian functions and the R_{back} as a third-order polynomial function[51]:

$$R_{peak1} = R_{peak1}^{max} \frac{(w_{peak1}/2)^2}{(w_{peak1}/2)^2 + \left(\Delta - \Delta_{peak1}\right)^2} \tag{3}$$

$$R_{peak2} = R_{peak2}^{max} \frac{(w_{peak2}/2)^2}{(w_{peak2}/2)^2 + \left(\Delta - \Delta_{peak2}\right)^2} \tag{4}$$

$$R_{back} = D0 + D1\,(\Delta - 2) + D2(\Delta - 2)^2 + D3(\Delta - 2)^3 \tag{5}$$

where w_{peak1} and w_{peak2} are the peak FWHM of the Lorentzian line-shape. The values of R_{peak1}^{max} and R_{peak2}^{max} refer to the true apparent relaxation rate. Chemical shift offsets are represented by Δ_{peak1} and Δ_{peak2}. The terms $D0$ to $D3$ are the zero-order to third-order polynomial coefficients.

A 2-step fitting strategy was applied to fit the Z-spectrum. The first step fits the background of the steady-state Z-spectrum Z^{ss}_{back} without the 2 CEST peaks (i.e., $R_{peak1} = R_{peak2} = 0$). Under the steady-state situation, the Z-spectrum Z^{ss}_{back} is correlated to R_{back} with Eq. 1 and is given by

$$Z^{ss}_{back} = \frac{cos^2\theta R_1}{R_{eff} + R_{back}} \tag{6}$$

Combining Eqs. 5 and 6, the Z^{ss}_{back} can be fitted by varying the polynomial coefficients $D0 - D3$. The second step fits the targeted peaks with the fixed background Z^{ss}_{back} (i.e., R_{back}). The fitting of Z^{ss} was accomplished by varying the parameters w_{peak1}/w_{peak2}, $\Delta_{peak1}/\Delta_{peak2}$, and $R^{max}_{peak1}/R^{max}_{peak2}$ according to

$$Z^{ss} = \frac{cos^2\theta R_1}{R_{eff} + R_{back} + R_{peak1} + R_{peak2}} \tag{7}$$

For the PCr and Cr mapping, the initial chemical shift offsets were set to 1.95 ppm and 2.5 ppm. The Z-spectrum between 1.3 ppm and 3.4 ppm was used for the 2-step fitting, and 3 regions of the Z-spectrum (i.e., 1.3-1.7 ppm, 2.25-2.35 ppm, and 2.83-3.4 ppm) were selected for the background fitting. Phosphocreatine is the main contributor to the CEST peak at 2.5 ppm, whereas the peak at 1.95 ppm contains both Cr and PCr. Therefore, the PCr signal rate (R^{max}_{PCr}) is given by the CEST peak at 2.5 ppm ($R^{max}_{2.5}$) (i.e., $R^{max}_{PCr} = R^{max}_{2.5}$), whereas the Cr signal (R^{max}_{Cr}) needs to be obtained by subtracting the PCr contribution from the 1.95-ppm CEST signal ($R^{max}_{1.95}$) using

$$R^{max}_{Cr} = R^{max}_{1.95} - F_{PCr} \cdot R^{max}_{2.5} \tag{8}$$

where F_{PCr} refers to the CEST signal ratio between the 2 peaks of the PCr CEST signal ($F_{PCr} = R^{max}_{PCr,1.95}/R^{max}_{PCr,2.5}$) and can be obtained from the Z-spectrum of the PCr phantom. The R^{max}_{Cr} and R^{max}_{PCr} can be correlated to the Cr and PCr concentrations ($[Cr]$ and $[PCr]$) obtained from MRS through the following relationship:

$$R^{max}_{Cr} = r_{Cr} \cdot [Cr] \tag{9}$$

$$R^{max}_{PCr} = r_{PCr} \cdot [PCr] \tag{10}$$

where r_{Cr} and r_{PCr} are the apparent relaxivities (expressed in $s^{-1}mM^{-1}$) of Cr and PCr, respectively, which are analogous to the relaxivity terms used for contrast agent studies. The normalized mean square error (NMSE) was used to objectively evaluate the goodness of the PLOF fit between the estimated and measured data, of which the definition is given as

$$NMSE = 1 - \frac{||S_{ref} - S_{fit}||^2}{||S_{ref} - mean(S_{ref})||^2} \tag{11}$$

where $||||$ indicates the 2-norm of a vector, S_{ref} refers to the observed CEST signals, and S_{fit} represents the fitting result obtained by the PLOF method. The value of NMSE varies between minus infinity (bad fit) to 1 (perfect fit).

The Cr and PCr concentrations from the in vivo ^{1}H MRS spectra were estimated using the LCModel method.[52,53] The tCr concentration was obtained from the ratio (g) between the area under a best-fit tCr spectrum in the LCModel on muscle and on the calibration phantom (20-mM Cr in cross-linked BSA) as $g \cdot 20mM$. Possible contributions of the Cr signals that are invisible in MRS due to binding effects with the cross-linked BSA were neglected in the current study. Taurine (Tau) is a high-concentration metabolite in muscle that shows strong and broad CEST signal around 2 ppm. Hence, the concentrations of Tau in both WT and GAMT-/- mice were also determined by MRS using the ratio between Tau and the tCr in the calibration phantom as obtained by the LCModel. Because of the overlap of the Cr and PCr signals in the proton spectrum, the concentration ratio between them is hard to determine by high-resolution in vivo ^{1}H MRS. In the literature, an approximate ratio of 1 : 3 has been reported for the Cr/PCr ratio in skeletal muscle (Cr 7.5 mM : PCr 22.5 mM).[53,54] This ratio was used for quantifying the Cr and PCr concentrations in this study.

The observed CEST signals at 2.5 ppm ($\Delta Z_{2.5}$) and 1.95 ppm ($\Delta Z_{1.95}$) were calculated by $\Delta Z_{2.5} = Z^{ss}_{back} - Z^{ss}_{2.5}$, $\Delta Z_{1.95} = Z^{ss}_{back} - Z^{ss}_{1.95}$. The observed amide proton peak ($\Delta Z_{3.6}$) was estimated by fitting the Z values at 3.1-3.2 ppm and 4.2-4.8 ppm using a first-order linear function. Then, the $\Delta Z_{3.6}$ was calculated by taking the difference between the fitted background (Z^{ss}_{back}) and the observed Z value at 3.6 ppm (i.e., $[Z^{ss}_{back} - Z^{ss}_{3.6}]$).

3 | RESULTS

3.1 | Magnetic resonance spectroscopy of the skeletal muscle

Typical in vivo ^{1}H MRS of the skeletal muscle of WT and GAMT-/- mice are shown in Figure 1. High-resolution T_2-weighted images by the rapid acquisition with refocused echoes sequence are included for anatomical guidance. From the spectra it can be seen that the tCr signals of the GAMT-/- skeletal muscle at 3 ppm and 3.9 ppm are significantly reduced compared with those of the WT mouse ($p < .001$). The tCr concentrations estimated by the LCModel method were 38.8 ± 2.8 mM and 1.2 ± 0.8 mM for the WT and GAMT-/- mice

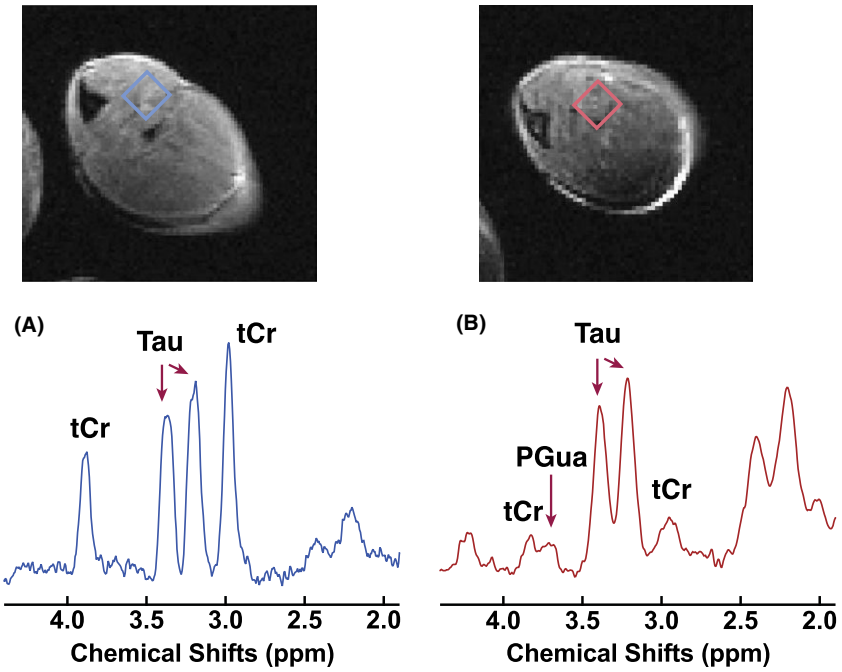

FIGURE 1 In vivo ^{1}H NMR spectra of the skeletal muscle of a wild-type (WT) mouse (A) and a guanidinoacetate N methyltransferase–deficient (GAMT-/-) mouse (B). The corresponding T_2-weighted images (rapid acquisition with refocused echoes sequence, in-plane resolution = 170 × 170 μm^2, slice thickness = 1.5 mm) are also shown. The rectangles indicated on the T_2-weighted images were selected as volumes of interest for the spectra. The assignment of the MRS peaks is also indicated. PGua, phosphorylated guanidinoacetate; Tau, taurine

($N = 3$), respectively. A weak and broad peak from PGua can be seen at 3.78 ppm.[42] The Tau concentrations were identical for the WT (58.3 ± 1.6 mM) and the GAMT-/- (58.3 ± 1.6 mM) mice.

3.2 | Z-spectra of the phantoms and the skeletal muscle

The Z-spectra of the 30-mM Cr, PCr, and Gua phantoms at pH = 7.0 recorded with 1-μT saturation power are shown in Figure 2A. There is one strong peak around 2.0 ppm present in the Cr CEST Z-spectrum, whereas 2 peaks around 2.0 ppm and 2.5 ppm are observed in the PCr CEST Z-spectrum. The PCr CEST signal around 2.5 ppm is about 3.0 ± 0.2% of the water magnetization, which is much stronger than the signal at 2 ppm (about 1.8 ± 0.2% of water magnetization). Using MTR_{asym} analysis, the contribution ratio F_{PCr} between the 2 peaks of the PCr CEST was determined to be 0.55 ± 0.02 (1.8 ± 0.2% : 3.0 ± 0.1%). The Cr CEST signal around 2 ppm (about 11.7 ± 0.5% of water proton magnetization) is far stronger than its PCr counterpart. For the CEST Z-spectrum of Gua, a strong CEST signal (12.5 ± 0.5%) can also be found at 2 ppm. The concentration dependencies of R_{Cr}^{max} (2 ppm) and R_{PCr}^{max} (2.5 ppm) were also determined from the Cr and PCr CEST effects in phantoms using Eq. 1 and the determined R_1. For these concentration studies in vitro (Figure 2B), both Cr and PCr R_{Cr}^{max} are linearly dependent on the concentration up to about 30 mM.

Figure 2C shows the comparison between the Z-spectra of the GAMT-/- and WT mice with a saturation power of 1 μT. To eliminate the mismatch of the Z-spectra due to the B_1 variation across the experiments, the Z-spectra were aligned on the intensity scale using the Z-spectral intensity at 5 ppm.[35] The MTC background change induced by B_1 inhomogeneity is approximately 2% of the water signal, which is comparable to the CEST contrasts of Cr and PCr. Hence, the intensity alignment was carried out to give a better comparison. The saturation offset was aligned using the signals around 0 ppm. Notable differences were observed for the Z-spectra of the GAMT-/- and WT mice between 1 and 3 ppm. The Z-spectrum of the WT mice showed 2 clear peaks around 1.95 ppm and 2.5 ppm, whereas there was only 1 sharp peak around 2.2 ppm in the Z-spectrum of the GAMT-/- mice. This confirms the observation by previous MRS studies on GAMT-/- mice that the concentration of Gua is negligible in the WT mouse muscle, whereas a high concentration of PGua is present in GAMT-/-.[42] The full Z-spectra of the GAMT-/- and WT mice with different saturation powers are shown in Figure 2D,E, respectively. As indicated, there are strong aliphatic peaks at the right side from 0 to –5 ppm with an approximate maximum peak around –3.6 ppm. The complicated line shape of this composite aliphatic peak may degrade the accuracy of the PCr and Cr quantification if one were to use the asymmetry analysis method, such as indicated in Figure 2F.

3.3 | Chemical exchange saturation transfer signal extraction and optimization

The fitting using the PLOF method is demonstrated in Figure 3A,B. The PLOF method fits the background and extracts the $R_{2.5}$ and $R_{1.95}$ curves. To determine the optimal saturation power for the in vivo Cr and PCr continuous-wave CEST experiments, the CEST signals at 3.6 ppm ($\Delta Z_{3.6}$), 2.5 ppm ($\Delta Z_{2.5}$), and 1.95 ppm ($\Delta Z_{1.95}$) were measured

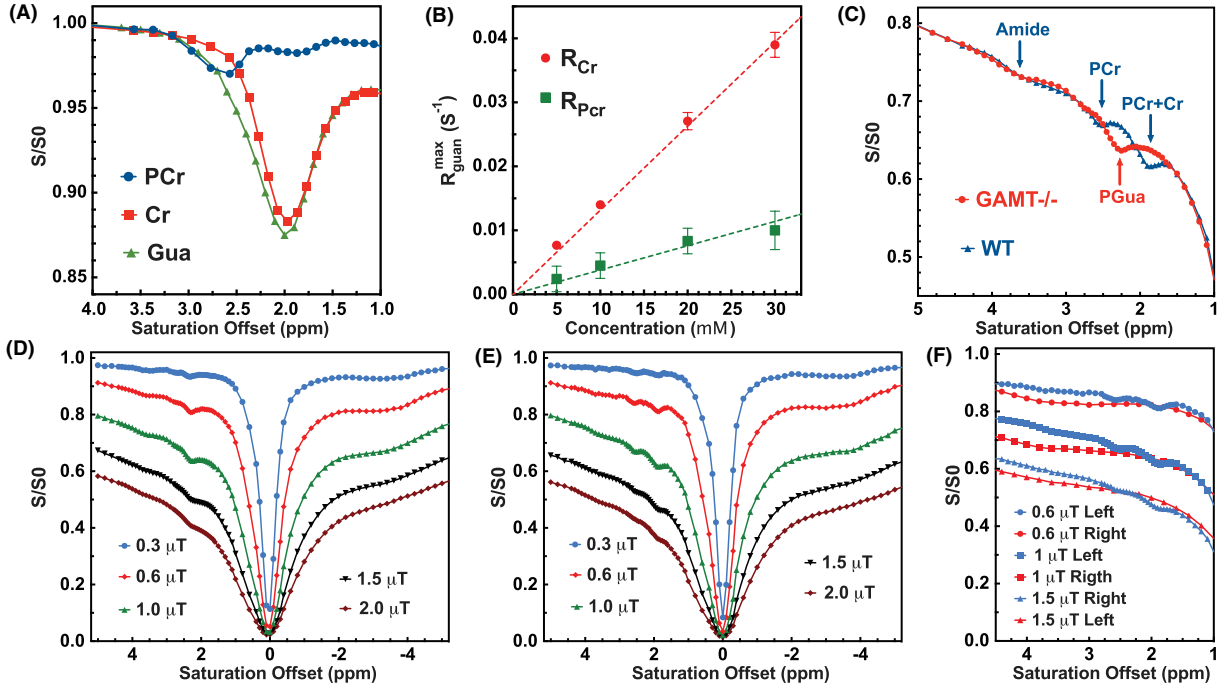

FIGURE 2 A, Z-spectra of 30-mM PCr (blue), Cr (red), and guanidinoacetate (Gua; green) solutions recorded using continuous-wave CEST with 1-μT saturation power and 3-second length. B, Concentration dependence of the Cr and PCr CEST signal R^{max}_{guan} at 2 ppm and 2.5 ppm, respectively. The values were obtained from peak intensities of the Cr/PCr resonances in the Z-spectra and the measured R_1 values (Eq. 1). The dashed lines ($y = 1.3 \times 10^{-3x}$ and $y = 3.8 \times 10^{-4x}$) are drawn for visual guidance of the linearity of the concentration dependence. C, Aligned averaged Z-spectra of GAMT-/- ($N = 3$) and WT mice ($N = 3$) collected with a saturation power of 1 μT (3-second length). The assignment of the CEST peaks is indicated. Typical full Z-spectra recorded on the calf muscle of the GAMT-/- mice (D) and the WT mice (E) using continuous-wave CEST with the saturation powers and lengths of 0.3 μT (4 seconds), 0.6 μT (4 seconds), 1 μT (3 seconds), 1.5 μT (3 seconds), and 2 μT (2 seconds). F, Comparisons of the left (1 ppm to 5 ppm, blue lines) and right (–1 ppm to –5 ppm, red lines) sides of Z-spectra recorded on the WT mice with saturation powers of 0.6 μT, 1 μT, and 1.5 μT. The right sides of the Z-spectra (–1 ppm to –5 ppm) were flipped to the positive side of Z-spectra for clarity

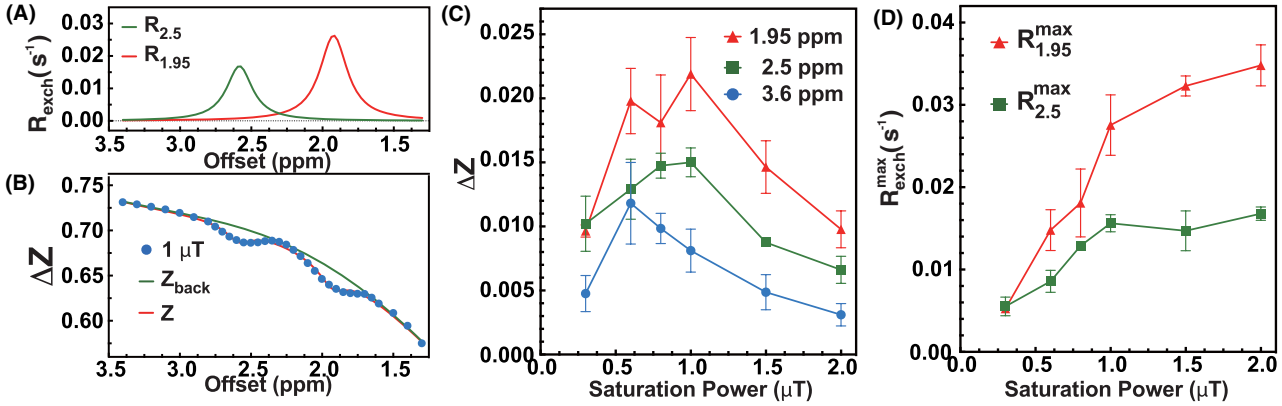

FIGURE 3 A, Typical $R_{2.5}$ and $R_{1.95}$ curves extracted using the 2-peak polynomial and Lorentzian line-shape fitting (PLOF) method. B, The corresponding fitting results (Z_{back} and Z) of Z-spectrum collected on a WT mouse ($R^2 = 0.9974$) with 1 μT saturation power. The frequency range between 1.3 and 3.4 ppm was used for the fitting, and 3 sections (i.e., 1.3-1.7 ppm, 2.25-2.35 ppm, and 2.83-3.4 ppm) were selected for the background fitting. C, Observed CEST signals (ΔZ) at 3.6 ppm, 2.5 ppm, and 1.95 ppm as a function of saturation power. D, Extracted $R^{max}_{2.5}$ and $R^{max}_{1.95}$ as a function of saturation power

as a function of saturation power (Figure 3C). The strongest $\Delta Z_{3.6}$ was observed at 0.6 μT with a maximum value around 1.2 ± 0.3% that dropped quickly with higher saturation power. At 1 μT, the $\Delta Z_{3.6}$ decreased to 0.8 ± 0.16% for muscle, which is much smaller than the $\Delta Z_{3.6}$ of mouse brain (1.55 ± 0.05%) at the same saturation power.[35] The maximum $\Delta Z_{2.5}$ and $\Delta Z_{1.95}$ were observed at about 1 μT. Similar to the tCr CEST study on mouse brain,[35] the observed CEST

signals at 2.5 ppm and 1.95 ppm quickly decreased with the increase in saturation power due to the spill-over from MTC and the other CEST signals. According to the theory of $R_{1\rho}$, the extracted $R_{1.95}^{max}$ and $R_{2.5}^{max}$ are immune to the spillover effect. As indicated in Figure 3D, the extracted $R_{1.95}^{max}$ values showed an increase with respect to saturation power, whereas the PCr signal $R_{2.5}^{max}$ increased first and then plateaued after 1 μT due to its much smaller exchange rate (i.e., fully labeled with saturation powers higher than 1 μT).

3.4 | Phosphocreatine and Cr concentration maps

The extracted $R_{1.95}^{max}$ and $R_{2.5}^{max}$ maps of skeletal muscle at a saturation power of 1 μT are shown in Figure 4B,C. The r_{Cr} and r_{PCr} were determined to be $2.85 \pm 0.05 \cdot 10^{-3}$ $s^{-1}mM^{-1}$ and $0.75 \pm 0.05 \cdot 10^{-3}$ $s^{-1}mM^{-1}$ at a saturation power of 1 μT, respectively. The concentration maps of Cr and PCr obtained using Eqs. 8 and 9 are shown in Figure 4D,E, respectively. The goodness of the PLOF fitting for each pixel is illustrated by the NMSE map shown in Figure 4F. The mean value and SD of the NMSE map are 0.9922 and 0.0034, respectively. The averaged Cr and PCr concentrations of the mouse calf muscle were determined to be 11.3 ± 1.4 mM and 30.8 ± 2.8 mM, respectively, which are slightly higher than the previously reported values (Cr 7.5 mM : PCr 22.5 mM) from spectroscopy.[42,54] Due to the relatively low resolution of the PCr and Cr maps, the maps are not following any pattern of muscle anatomy. Also, the edges of the PCr and Cr maps (transition from muscle to air) show strong concentration gradients due to the partial volume effect.

4 | DISCUSSION

The current study demonstrates the use of a 2-peak PLOF method to yield PCr and Cr concentration maps. The Z-spectra in Figure 2 and the analysis of the results in Figure 3 indicate that a mobile protein guanidium peak is undetectable and the amide peak is small with a maximum amplitude of approximately 1.2% of water magnetization in skeletal muscle. This is quite different from the previous brain studies, in which amide and guanidinium peaks are commonly observed due to the abundance of mobile proteins in brain tissue. The disappearance of the protein guanidinium peak and the reduction of the amide peaks from the proteins are favorable to the extraction of clean Cr and PCr CEST signal. The skeletal muscle Z-spectrum between 0 and –3.6 ppm was still dominated by the relayed nuclear Overhauser effect signal arising from the aliphatic protons of glycogen, proteins, and lipids.

The extraction of Cr and PCr CEST signal provides an opportunity to optimize the acquisition scheme for in vivo

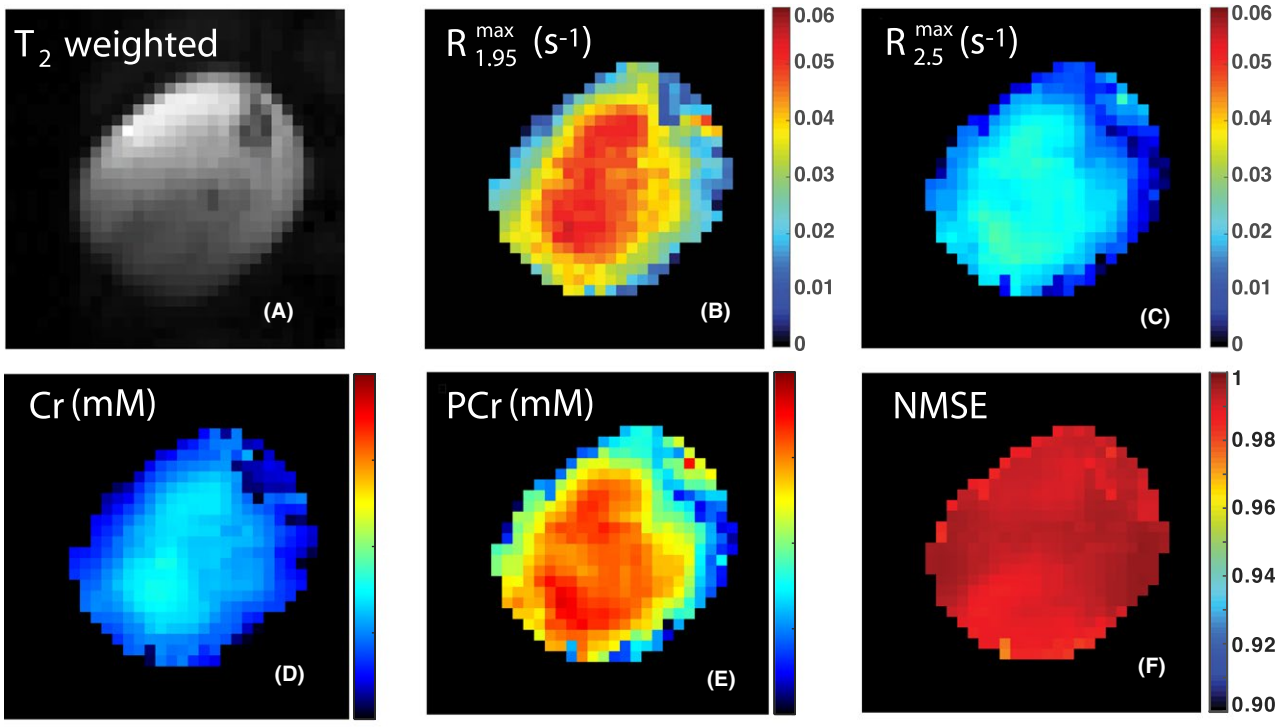

FIGURE 4 A, T_2-weighted image of the mouse hind leg used for anatomical guidance. The extracted maps of $R_{1.95}^{max}$ (B) and $R_{2.5}^{max}$ (C) determined by the PLOF method using the Z-spectrum recorded with a saturation power of 1 μT. The Cr (D) and PCr (E) concentration maps calculated using Eqs. 9 and 10, respectively. F, Normalized mean square error (NMSE) map calculated using Eq. 11 for evaluating the PLOF fitting

Cr and PCr CEST applications at 11.7 T. This study, together with the previous mouse brain study,[35] demonstrates that the observed CEST signals of PCr and Cr in tissues are different from those in phantoms. After reaching a maximum value at 1 μT, the observed muscle PCr and Cr CEST signals quickly decreased with an increase in saturation power, as shown in Figure 3. However, for the phantom studies, the PCr and Cr CEST signals increased when the saturation power rose above 1 μT.[38] This phenomenon can be explained by the spillover effect induced by the background signals from direct saturation and semisolid MTC effects, as indicated in the previous study[35]:

$$\Delta Z_{obs} = {Z^{ss}_{back}}^2(1-Z_{clean}) \quad (12)$$

where $(1-Z_{clean})$ is the clean CEST signal without MTC and direct saturation, and ΔZ_{obs} is the observed PCr or Cr CEST signal. For the Cr/PCr CEST signals, the saturation efficiency is proportional to the saturation power initially, and then levels off slowly until reaching maximum saturation (Figure 3D). However, the MTC increases stronger with saturation powers, leading to a decrease in Z^{ss}_{back}. As a result, the observed CEST signal will drop quickly at higher saturation powers, as predicted in Eq. 11. A similar power dependence of CEST signal has also been observed for other slow-exchanging protons, such as relayed nuclear Overhauser effect CEST.[41]

The SNR of the PCr and Cr CEST (SNR_{CEST}) can be estimated by the CEST signal ($\Delta Z_{Cr/PCr}$) and the SD of the residual fitting signal from the PLOF method (Std_{PLOF}) using $SNR_{CEST} = \Delta Z_{Cr/PCr}/Std_{PLOF}$. The residual fitting signal was extracted from the region between 2.9 ppm and 3.5 ppm by subtracting the fitted Z^{ss} and the experimental Z-spectrum. The SNR_{CEST} values were found to be 38.5 and 19.5 for Cr and PCr for a voxel volume of 8 mm^3 (slice thickness = 1.5 mm and region of interest = 5.3 mm^2), respectively. As a comparison, the SNR values for the Cr and PCr peak measured by MRS with same voxel volume ($2 \times 2 \times 2$ mm^3) and a same experimental time as CEST experiments (5 minutes) were 2.6 ± 0.5 and 8 ± 0.5, respectively. Therefore, the SNR gain using CEST is about 14.8 times higher than the MRS method for Cr, whereas PCr is about 2.4 times higher. The CEST SNR can be further improved by either applying a more stable image acquisition module or optimizing the CEST labeling scheme.

The proposed PLOF method is ready to be transferred directly to 7T MRI scanners. However, we expect some challenges when applying PLOF to simultaneously obtain PCr and Cr maps on 3T scanners. Because of the fast exchange rate of guanidinium protons in Cr, the CEST signal at 2 ppm is broad and starting to coalesce with the water peak. The detection of PCr on 3T systems is possible due to its relatively slow guanidinium proton exchange rate (120 ± 50 Hz) and larger offset difference with water. The saturation power therefore needs to be reduced at 3 T and, in consideration of the water direct saturation, a saturation power between 0.5 μT and 0.7 μT and a duration between 800 ms and 1 second is estimated to be suitable for PCr CEST experiments on a 3T scanner. We attribute the lack of a PCr signal in previous CEST studies[15] at 3 T to the strong saturation power applied. With strong saturation power, the CEST peaks of PCr and Cr merge with each other and the background MTC, direct saturation, and glycogen signals and appear to be 1 broad CEST signal. Due to the faster exchange rate of guanidinium proton in Cr, the CEST contrast of Cr is much stronger compared with that of PCr at the same concentration. Therefore, although both PCr and Cr contribute to MTR_{asym} signal at 2 ppm, the signal change during leg exercise is dominated by the Cr.

5 | CONCLUSIONS

In this study, skeletal-muscle PCr and Cr CEST signal concentrations were determined by comparing Z-spectra recorded on WT and GAMT-/- mice. The CEST peak at 1.95 ppm contains contributions from both Cr and PCr, whereas the CEST peak at 2.5 ppm is primarily the result of PCr. The CEST signal originating from protein guanidinium protons is not detectable in skeletal muscle, which is favorable for the extraction of clean PCr and Cr CEST signals. The PCr and Cr maps of skeletal muscle could be obtained simultaneously using the proposed PLOF method.

ACKNOWLEDGMENTS

This work was supported by NIH grants R01EB015032, P41EB015909, and R01HL63030. The authors thank Dirk Isenbrandt for creating and providing the GAMT-/- mice.

REFERENCES

1. Wyss M, Kaddurah-daouk R. Creatine and creatinine metabolism. *Physiol Rev*. 2000;80:1107.
2. Andres RH, Ducray AD, Schlattner U, Wallimann T, Widmer HR. Functions and effects of creatine in the central nervous system. *Brain Res Bull*. 2008;76:329–343.
3. Schlattner U, Tokarska-Schlattner M, Wallimann T. Mitochondrial creatine kinase in human health and disease. *Biochim Biophys Acta*. 2006;1762:164–180.
4. Boesch C. Musculoskeletal spectroscopy. *J Magn Reson Imaging*. 2007;25:321–338.
5. Bottomley PA, Lee Y, Weiss RG. Total creatine in muscle: imaging and quantification with proton MR spectroscopy. *Radiology*. 1997;204:403–410.
6. Prompers JJ, Jeneson JA, Drost MR, Oomens CC, Strijkers GJ, Nicolay K. Dynamic MRS and MRI of skeletal muscle function and biomechanics. *NMR Biomed*. 2006;19:927–953.

7. Kemp GJ, Meyerspeer M, Moser E. Absolute quantification of phosphorus metabolite concentrations in human muscle in vivo by 31P MRS: a quantitative review. *NMR Biomed*. 2007;20:555–565.
8. Wolff S, Balaban R. NMR imaging of labile proton exchange. *J Magn Reson*. 1990;86:164–169.
9. van Zijl P, Yadav NN. Chemical exchange saturation transfer (CEST): What is in a name and what isn't? *Magn Reson Med*. 2011;65:927–948.
10. vanZijl P, Lam WW, Xu J, Knutsson L, Stanisz GJ. Magnetization transfer contrast and chemical exchange saturation transfer MRI. Features and analysis of the field-dependent saturation spectrum. *NeuroImage*. 2018;168:222–241.
11. Liu G, Song X, Chan KW, McMahon MT. Nuts and bolts of chemical exchange saturation transfer MRI. *NMR Biomed*. 2013;26:810–828.
12. Jones KM, Pollard AC, Pagel MD. Clinical applications of chemical exchange saturation transfer (CEST) MRI. *J Magn Reson Imaging*. 2018;47:11–27.
13. van Zijl P, Sehgal AA. *Proton chemical exchange saturation transfer (CEST) MRS and MRI. eMagRes*. 2016;5:1–26.
14. Haris M, Nanga RP, Singh A, et al. Exchange rates of creatine kinase metabolites: feasibility of imaging creatine by chemical exchange saturation transfer MRI. *NMR Biomed*. 2012;25:1305–1309.
15. Haris M, Singh A, Cai K, et al. A technique for in vivo mapping of myocardial creatine kinase metabolism. *Nat Med*. 2014;20:209–214.
16. Zu Z, Louie EA, Lin EC, et al. Chemical exchange rotation transfer imaging of intermediate-exchanging amines at 2 ppm. *NMR Biomed*. 2017;30.;. https://doi.org/10.1002/nbm.3756.
17. Zhou J, Payen JF, Wilson DA, Traystman RJ, van Zijl PC. Using the amide proton signals of intracellular proteins and peptides to detect pH effects in MRI. *Nat Med*. 2003;9:1085–1090.
18. van Zijl PC, Jones CK, Ren J, Malloy CR, Sherry AD. MRI detection of glycogen in vivo by using chemical exchange saturation transfer imaging (glycoCEST). *Proc Natl Acad Sci U S A*. 2007;104:4359–4364.
19. Cai K, Haris M, Singh A, et al. Magnetic resonance imaging of glutamate. *Nat Med*. 2012;18:302–306.
20. Ling W, Regatte RR, Navon G, Jerschow A. Assessment of glycosaminoglycan concentration in vivo by chemical exchange-dependent saturation transfer (gagCEST). *Proc Natl Acad Sci U S A*. 2008;105:2266–2270.
21. Jin T, Wang P, Zong X, Kim S-G. Magnetic resonance imaging of the Amine-Proton EXchange (APEX) dependent contrast. *NeuroImage*. 2012;59(2):1218–1227.
22. Zong X, Wang P, Kim SG, Jin T. Sensitivity and source of amine-proton exchange and amide-proton transfer magnetic resonance imaging in cerebral ischemia. *Magn Reson Med*. 2014;71(1):118–132.
23. Davis KA, Nanga RP, Das S, et al. Glutamate imaging (GluCEST) lateralizes epileptic foci in nonlesional temporal lobe epilepsy. *Sci Transl Med*. 2015;7:309ra161.
24. Chen L, Xu X, Zeng H, et al. Separating fast and slow exchange transfer and magnetization transfer using off-resonance variable delay multiple pulse (VDMP) MRI. *Magn Reson Med*. 2018;80:1568–1576.
25. Zaiss M, Windschuh J, Goerke S, et al. Downfield-NOE-suppressed amide-CEST-MRI at 7 Tesla provides a unique contrast in human glioblastoma. *Magn Reson Med*. 2017;77:196–208.
26. Haris M, Singh A, Cai K, et al. MICEST: a potential tool for non-invasive detection of molecular changes in Alzheimer's disease. *J Neurosci Methods*. 2013;212:87–93.
27. Zhang XY, Wang F, Afzal A, et al. A new NOE-mediated MT signal at around -1.6 ppm for detecting ischemic stroke in rat brain. *Magn Reson Imaging*. 2016;34:1100–1106.
28. Jones CK, Huang A, Xu J, et al. Nuclear Overhauser enhancement (NOE) imaging in the human brain at 7T. *NeuroImage*. 2013;77C:114–124.
29. Xu J, Yadav NN, Bar-Shir A, et al. Variable delay multi-pulse train for fast chemical exchange saturation transfer and relayed-nuclear overhauser enhancement MRI. *Magn Reson Med*. 2014;71:1798–1812.
30. Cai K, Singh A, Poptani H, et al. CEST signal at 2 ppm (CEST@2ppm) from Z-spectral fitting correlates with creatine distribution in brain tumor. *NMR Biomed*. 2015;28:1–8.
31. Desmond KL, Moosvi F, Stanisz GJ. Mapping of amide, amine, and aliphatic peaks in the CEST spectra of murine xenografts at 7 T. *Magn Reson Med*. 2014;71:1841–1853.
32. Zu Z, Janve VA, Xu J, Does MD, Gore JC, Gochberg DF. A new method for detecting exchanging amide protons using chemical exchange rotation transfer. *Magn Reson Med*. 2013;69:637–647.
33. Zu Z, Janve VA, Li K, Does MD, Gore JC, Gochberg DF. Multi-angle ratiometric approach to measure chemical exchange in amide proton transfer imaging. *Magn Reson Med*. 2012;68:711–719.
34. Zu Z, Lin E, Louie E, et al. *Chemical exchange rotation transfer imaging of phosphocreatine in muscle*. In: Proceedings of the 26th Annual Meeting of ISMRM, Paris, France; 2018:5106.
35. Chen L, Zeng H, Xu X, et al. Investigation of the contribution of total creatine to the CEST Z-spectrum of brain using a knockout mouse model. *NMR Biomed*. 2017;30:e3834.
36. Zhang XY, Xie J, Wang F, et al. Assignment of the molecular origins of CEST signals at 2 ppm in rat brain. *Magn Reson Med*. 2017;78:881–887.
37. Kogan F, Haris M, Debrosse C, et al. In vivo chemical exchange saturation transfer imaging of creatine (CrCEST) in skeletal muscle at 3T. *J Magn Reson Imaging*. 2014;40:596–602.
38. Rerich E, Zaiss M, Korzowski A, Ladd ME, Bachert P. Relaxation-compensated CEST-MRI at 7 T for mapping of creatine content and pH—preliminary application in human muscle tissue in vivo. *NMR Biomed*. 2015;28:1402–1412.
39. Jin T, Autio J, Obata T, Kim S-G. Spin-locking versus chemical exchange saturation transfer MRI for investigating chemical exchange process between water and labile metabolite protons. *Magn Reson Med*. 2011;65:1448–1460.
40. Zaiss M, Bachert P. Chemical exchange saturation transfer (CEST) and MR Z-spectroscopy in vivo: a review of theoretical approaches and methods. *Phys Med Biol*. 2013;58:R221–R269.
41. Yadav NN, Yang X, Li Y, Li W, Liu G, van Zijl P. Detection of dynamic substrate binding using MRI. *Sci Rep*. 2017;7:10138.
42. Renema WK, Schmidt A, van Asten JJ et al. MR spectroscopy of muscle and brain in guanidinoacetate methyltransferase (GAMT)-deficient mice: validation of an animal model to study creatine deficiency. *Magn Reson Med*. 2003;50:936–943.
43. Skelton MR, Schaefer TL, Graham DL, et al. Creatine transporter (CrT; Slc6a8) knockout mice as a model of human CrT deficiency. *PLoS One*. 2011;6:e16187.
44. Schulze A. Creatine deficiency syndromes. *Handb Clin Neurol*. 2013;113:1837–1843.

45. Stockler S, Holzbach U, Hanefeld F, et al. Creatine deficiency in the brain: a new, treatable inborn error of metabolism. *Pediatr Res*. 1994;36:409–413.
46. Kan HE, Meeuwissen E, van Asten JJ, Veltien A, Isbrandt D, Heerschap A. Creatine uptake in brain and skeletal muscle of mice lacking guanidinoacetate methyltransferase assessed by magnetic resonance spectroscopy. *J Appl Physiol*. 2007;102:2121–2127.
47. Zaiss M, Bachert P. Exchange-dependent relaxation in the rotating frame for slow and intermediate exchange—modeling off-resonant spin-lock and chemical exchange saturation transfer. *NMR Biomed*. 2013;26:507–518.
48. Xu J, Zaiss M, Zu Z, et al. On the origins of chemical exchange saturation transfer (CEST) contrast in tumors at 9.4 T. *NMR Biomed*. 2014;27:406–416.
49. Zaiss M, Xu J, Goerke S, et al. Inverse Z-spectrum analysis for spillover-, MT-, and T1 -corrected steady-state pulsed CEST-MRI—application to pH-weighted MRI of acute stroke. *NMR Biomed*. 2014;27:240–252.
50. Ryoo D, Xu X, Li Y, et al. Detection and quantification of hydrogen peroxide in aqueous solutions using chemical exchange saturation transfer. *Anal Chem*. 2017;89:7758–7764.
51. Lauzon CB, van Zijl P, Stivers JT. Using the water signal to detect invisible exchanging protons in the catalytic triad of a serine protease. *J Biomol NMR*. 2011;50:299–314.
52. Provencher SW. Estimation of metabolite concentrations from localized in vivo proton NMR spectra. *Magn Reson Med*. 1993;30:672–679.
53. Provencher SW. Automatic quantitation of localized in vivo 1H spectra with LCModel. *NMR Biomed*. 2001;14:260–264.
54. in't Zandt HJA, de Groof AJC, Renema WKJ, et al. Presence of (phospho) creatine in developing and adult skeletal muscle of mice without mitochondrial and cytosolic muscle creatine kinase isoforms. *J Physiol*. 2003;548:847–858.

How to cite this article: Chen L, Barker PB, Weiss RG, van Zijl PCM, Xu J. Creatine and phosphocreatine mapping of mouse skeletal muscle by a polynomial and Lorentzian line-shape fitting CEST method. *Magn Reson Med.* 2018;00:1–10. https://doi.org/10.1002/mrm.27514